PAPER

Nanosheet Molding Method to Estimate the Size of Bilayers Suspended in Liquid

Received 00th January 20xx,
Accepted 00th January 20xx

DOI: 10.1039/x0xx00000x

Koki Sasaki, Jose A. Hernandez Gaitan, Yuki Tokuda, Koji Miyake, Yoshiaki Uchida,* and Norikazu Nishiyama

Various methods have been developed to determine the size of molecular bilayer structures dispersed in liquids. We focused on the nanosheet (NS) growth inside the bilayers in hyperswollen lamellar (HL) phases. Here, we propose the method to evaluate the size of bilayers in liquid by observing palladium NSs (PdNSs) growing rapidly in the bilayers of the HL phase. It uncovered that the width of PdNSs depends on methanol concentration, on which the stability of the HL phase also depends. Considering that the stability of the HL phase is positively correlated with the width of bilayers, we concluded that the observation of PdNSs probably corresponds to the indirect measurement of the width of bilayers. This method will also be applied to various other bilayers. Moreover, the PdNSs with a few nanometers of thickness and several hundred nanometers of width show higher catalytic activity for the reduction reaction of 4-nitrophenol to 4-aminophenol than the previously reported Pd catalysts without any supports.

Introduction

Bilayers suspended in liquids like vesicles[1] and freestanding bilayers[2] are important objects in physical science, life science, and biomedical engineering.[3-5] Their shapes and stability strongly correlated with their properties should be clarified because they are used for the model of cell membranes,[5] drug delivery systems (DDS),[6] toxicity screening,[7] and separation membranes.[8] Their deformation, fusion, and aggregation easily occur in response to various stimuli: pH, compositions, temperature, and shear stress.[9–18] Despite the desire to understand their behavior, it is impossible to directly measure the size of such stimuli-sensitive bilayer structures in situ.

Various methods have been developed to determine the size and polydispersity of bilayer structures. Due to its usability and applicability, the dynamic light scattering (DLS) technique is the most popular method, as shown in Fig. 1a.[19,20] It measures the size of objects from a few nanometers to a few micrometers in situ. However, it is not good at estimating the shape of the objects. Although transmission electron microscopy (TEM), cryogenic-TEM (cryo-TEM), and atomic force microscopy (AFM) are powerful tools to measure the size and shape simultaneously,[20–22] they cannot observe the dispersion state in situ because they are frozen or immobilized on a substrate, as shown in Fig. 1b. Copying the shape of the bilayers to some solid material in the solution in situ could solve the dilemma.

We focused on the nanosheet (NS) growth inside the bilayers in hyperswollen lamellar (HL) phases, as shown in Fig. 1c.[23–28] The HL phase consists of suspended bilayers with several nm thicknesses that keep several hundred nm intervals with each other.[29,30] Although literature explains that large fluctuations of bilayers stabilize HL phases, the actual dynamic behavior of the bilayers, such as association and dissociation, has not been clarified yet. The bilayers can offer thin two-dimensional (2-D) reaction fields. This soft-templating method is named the 'two-dimensional reactor in amphiphilic phase (TRAP) method.' In the TRAP method, the width of NSs growing inside the bilayers is proportional to that of the bilayers.[26, 28] The width of NSs can be controlled using the Reynolds number because the excess internal elastic stress stabilizes the HL phase and expands the area of bilayers.[31] We guess that the dynamic behavior of the bilayers could be discussed by observing the size of NSs growing inside the bilayers.

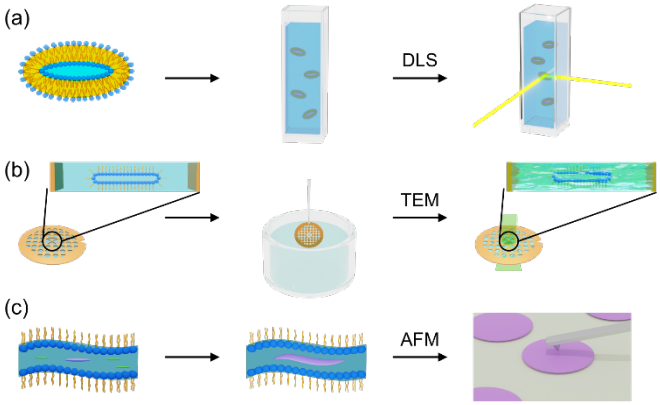

Fig.1 Schematic illustration of the evaluation method of the size and polydispersity of bilayers. (a) DLS technique. It gives the isotropic size distribution for the bilayers dispersed in liquids. (b) Cryo-TEM. It observes the sample frozen on the substrate. (c) The present evaluation method. It measures the size of the bilayers by observing nanosheets growing inside bilayers using AFM.

Graduate School of Engineering Science, Osaka University, 1-3 Machikaneyama-cho, Toyonaka, Osaka 560-8531, Japan

†Electronic Supplementary Information (ESI) available: [details of any supplementary information available should be included here]. See DOI: 10.1039/x0xx00000x

The snapshot molding where NSs copy the shape of bilayers requires materials rapidly growing in the bilayers; palladium (Pd) could be suitable because of its high growth rate. Moreover, Pd is promising as the material for NSs with high specific surface areas due to its superior applications, such as catalysis,[32] hydrogen production,[33] fuel cells,[34] and sensors.[35] Among the catalytic activity for many reactions like oxidation and coupling reactions, Pd metal shows high catalytic activity for the reductions occurring at the surface.[36] Pd NSs (PdNSs) should show higher catalytic activity than the others because of their large surface area.[37–40]

Here, we report the method to measure the size of bilayers in the HL phase of TRAP solutions by observing PdNSs growing in the bilayers. We display that the stability of the HL phase changes in sync with the size of bilayers by measuring the size of the synthesized PdNSs when the cosurfactant concentration changes. We also demonstrate the catalytic activity of the obtained PdNSs for the reduction reaction of 4-nitrophenol (4-NP) to 4-aminophenol (4-AP).

Experimental

Chemicals

Heptane, methanol, and hydrogen hexachloroplatinate (IV) hexahydrate (K_2PdCl_6) were purchased from Wako Pure Chemical Industries Co. Sodium borohydride ($NaBH_4$) was purchased from Tokyo Chemical Industry Co., Ltd. Brij L4 was purchased from Merck KGaA. The water with a resistivity of 18.2 MΩ cm was obtained from a water purifier (Direct-Q UV, Millipore Co.).

Characterization

The crystal structures were estimated from X-ray diffraction (XRD) patterns collected using a PANalytical X'Pert PRO diffractometer with Cu Kα radiation, operated at 45 kV and 40 mA. The scan range (2θ) was from 30° to 90° at a sweep rate of $0.10^{o}s^{-1}$. The size distributions of PdNSs were measured by dynamic light scattering (DLS) using ELSZ-2000 (Otsuka Electronics Co., Ltd.) at 25°C. The samples were suspended in ethanol for the DLS measurement. Transmission electron microscopy (TEM) images were obtained using a Hitachi H-800 at 200 kV. Atomic force microscopy (AFM) images were taken using a Veeco Instruments MMAFM-2. The samples were deposited on freshly exfoliated mica sheets as substrates for the AFM measurements. We measured 30 objects for each sample and calculated the average and standard deviation of the size and thickness, respectively. Decomposition temperature was measured by thermo-gravimetry (TG) analysis using DTG-60 (Shimadzu Co.) under nitrogen with a continuous flow rate of 60 mL min^{-1}. The samples were heated from room temperature to 600°C at a heating rate of 20°C min^{-1}.

Synthesis of palladium nanosheets

PdNSs were synthesized in the HL phases. The heptane solution (21 mL) of K_2PdCl_6 (1.0×10^{-1} wt%), Brij L4 (6.9 wt%), water (1.9 wt%), and methanol (1.0 wt%) and the heptane solution (21 mL) of $NaBH_4$ (2.6×10^{-2} wt%), Brij L4 (6.9 wt%), sodium hydroxide solution (pH 11) (1.9 wt%), and methanol (1.0 wt%) were separately prepared. A TRAP solution dissolving $NaBH_4$ was poured into another TRAP solution dissolving K_2PdCl_6 under stirring (300 rpm). The final products were centrifuged at 11,000 rpm for 30 min and washed three times with ethanol.

Synthesis of fine palladium particles

Fine palladium particles were synthesized in a heptane solution (42 mL) of K_2PdCl_6 (1.1×10^{-1} wt%), water (2.0 wt%), and methanol (1.1 wt%). The solution was poured into a 100 mL beaker and stirred (300 rpm). Another heptane solution (42 mL) of $NaBH_4$ (2.9×10^{-2} wt%), sodium hydroxide solution (pH 11) (2.0 wt%), and methanol (1.1 wt%) was added to the same 100 mL beaker. The final products were centrifuged at 11,000 rpm for 30 min and washed three times with ethanol.

Catalytic reaction test

Catalytic reactions were performed in a standard 3.5 mL quartz cuvette with a 10 mm path length. Typically, a total of 0.1 mL water was mixed with 1.7 mL aqueous 4-NP solution (2.0×10^{-4} mol L^{-1}) and 1 mL of freshly prepared aqueous $NaBH_4$ solution (1.5×10^{-2} mol L^{-1}) in a standard quartz cuvette. Then the Pt catalyst (0.2 mL, 1 mg mL^{-1}) was rapidly added to the quartz cell to trigger the catalytic reaction. The ultraviolet-visible (UV-Vis) spectroscopy was employed to monitor the conversion process of 4-NP to 4-AP by recording the time-dependent absorption spectra of the reaction mixtures using V-570 (JASCO Co.). The UV-vis absorbance spectra were recorded at 2 min intervals in the range of 250–500 nm.

Results and discussion

First, we examined if the HL phases are stable even with the ingredients of PdNSs. Since the birefringence reflects the stability of HL phases for the TRAP solutions, we can easily test the stability by observing it using a polarizing film wrapped around the vessel, as shown in Fig. 2a.[26] The polarized photograph of the TRAP solution consisting of heptane (90.1 wt%), Brij L4 (6.9 wt%), water (1.9 wt%), and methanol (1.0 wt%) shows birefringence typical of HL phases, as shown in Fig. 2b.[28] We separately added potassium tetrachloropalladate (II) (K_2PdCl_4) and sodium borohydride ($NaBH_4$) to the TRAP solutions in two vessels. The two TRAP solutions with each ingredient maintained a birefringence typical of HL phases, as shown in Fig. 2c and 2d. These results indicate that the hydrophilic TRAPs are likely to trap K_2PdCl_4 and $NaBH_4$ stably and that their addition did not affect the stability of the HL phases.

Then, we tried synthesizing PdNSs by pouring a TRAP solution dissolving $NaBH_4$ into another TRAP solution dissolving K_2PdCl_4. After stirring the mixed TRAP solution for 15 min, we centrifuged the reaction mixture at 11000 rpm for 30 min and washed the black precipitate three times with ethanol. The thermogravimetric (TG) analysis of the obtained black powder did not show weight reduction between 200 °C and 400 °C, in which Brij L4 shows weight reduction, as shown in Fig. S1. The

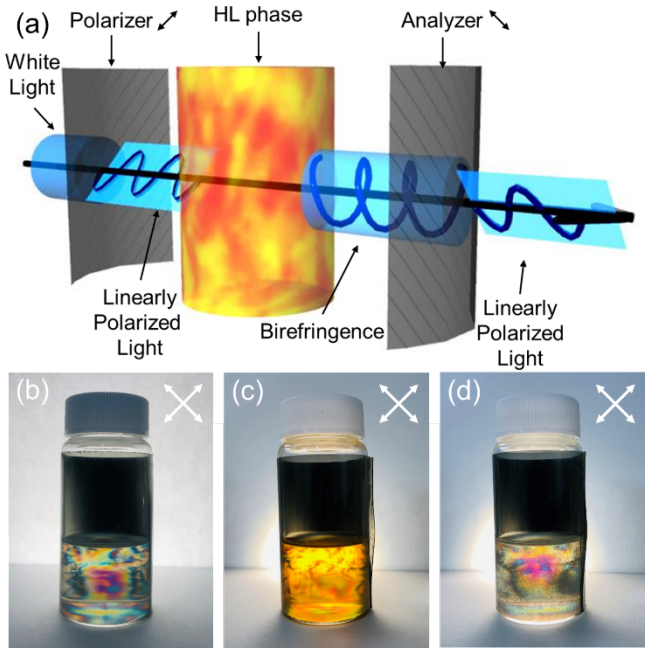

Fig. 2 Observation of birefringence of the heptane solution of Brij L4 containing water. (a) The optical system to take polarized photographs of hyperswollen lyotropic lamellar phases. A polarizing film is wrapped around a vessel while tilted at 45°. Polarized photographs of (b) TRAP solution of heptane (90.1 wt%), water (1.9 wt%), Brij L4 (6.9 wt%) and methanol (1.0 wt%), (c) TRAP solution of heptane (90.1 wt%), water (1.9 wt%), Brij L4 (6.9 wt%), methanol (1.0 wt%) and K_2PdCl_4 (1.0×10^{-1} wt%), and (d) TRAP solution of heptane (90.2 wt%), sodium hydroxide solution (pH 11) (1.9 wt %), Brij L4 (6.9 wt %), methanol (1.0 wt %), and $NaBH_4$ (2.7×10^{-2} wt %).

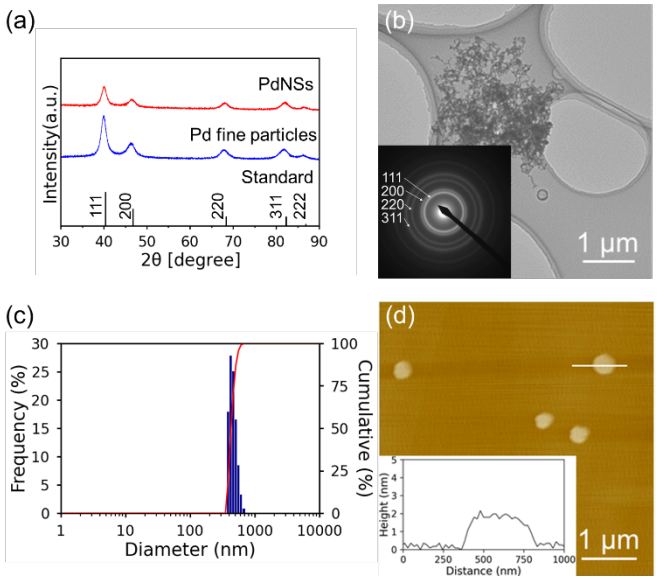

Fig. 3 Characterization of PdNSs synthesized in a TRAP solution with 1.0 wt% methanol. (a) XRD patterns of the PdNSs (red), Pd fine particles (blue) and a standard XRD pattern of Pd (black). (b) DLS analysis of PdNSs. (c) TEM photograph of PdNSs, and SAED pattern of PdNSs. (d) AFM photograph and cross-section of one of the synthesized PdNSs.

amphiphile Brij L4 does not seem to cover the products. The X-ray diffraction (XRD) pattern of the black powder is shown in Fig. 3a. The peak positions and intensity ratios of the synthesized powder are well fitted to those of Pd fine particles, which were synthesized in the heptane solution without Brij L4. This result indicates that the black powder is metallic Pd, and each crystallite grows isotropically. The full width at half-maximum (FWHM) of each of the XRD peaks for the obtained black powder is shown in Table S1. The Williamson-Hall plots indicate that the crystallite size of the obtained powder is smaller than that of Pd fine particles, as shown in Fig. S2.

We estimated the particle size distributions for the obtained powder by dynamic light scattering (DLS) measurements, as shown in Fig. 3b. The sharp peak indicates the absence of the aggregates. The transmission electron microscopy (TEM) photographs show sheet-like particles. The selected area electron diffraction (SAED) patterns indicate that the sample does not contain impurities, as shown in Figs. 3c and S3. The concentric circles of the SAED patterns also indicates that the sheet-like particles are composed of small crystallites. The confined thin two-dimensional (2-D) reaction field of the HL phase promotes the lateral bonding of the uniformly nanosized Pd platelets.[26] The horizontal width and thickness of the products measured by atomic force microscopy (AFM) are 485 ± 65 and 2.18 ± 0.40 nm, respectively, as shown in Fig. 3e. These results indicate that the obtained products are freestanding PdNSs.

We observed the TRAP solutions dissolving methanol with concentrations from 0 wt% to 2.24 wt%, as shown in Fig. 4a. The birefringence depends on the methanol concentration (w_{Me}). The stable HL phase shows colorful birefringence without stirring, whereas the metastable HL phase shows black and white birefringence only with stirring.[28] The TRAP solutions with methanol concentrations between 0.40 wt% and 1.66 wt% show birefringence derived from the anisotropy of the HL phases. In particular, the TRAP solutions with methanol concentrations between 1.00 wt% and 1.46 wt% exhibit stable HL phases.[28,31]

We measured the size dependence of the obtained PdNSs on w_{Me} using AFM, as shown in Table S2 and Fig. S4. The thickness of PdNSs looks independent of w_{Me} when w_{Me} is between 0.17 wt% and 2.24 wt%, whereas the thickness of PdNSs becomes thick when w_{Me} is 0 wt% (product **1**) as shown in Fig. 4c. The width of PdNSs is positively correlated with the strength of the birefringence of the HL phase, as shown in Fig. 4b. It suggests that the width of bilayers is also positively correlated with stability of HL phase. The width of products **6**, **7**, and **8** obtained at the stable state depends on w_{Me}. Methanol seems to stabilize the HL phase by swelling the hydrophilic part to enlarge the bilayers. Moreover, the excess amount of methanol destabilizes the HL phase; product **8** is smaller than product **7**. Moreover, we noticed that the standard deviation depends on w_{Me}. It would be useful to discuss the dynamics of bilayers.

The widths of products **6**-**8** synthesized in the stable HL phases have larger standard deviations than the others. The number of nanoplatelets used for the NS formation is non-uniform. Meanwhile, their thicknesses have small standard deviations. These results suggest that the bilayers laterally stick together and come apart, as shown is Fig. S5a. Similar explanations are possible for the dynamics of TRAPs in other

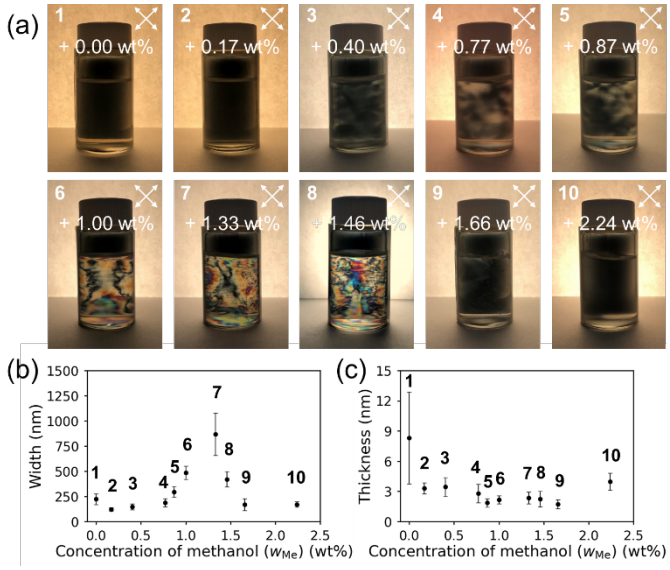

Fig. 4 Dependence of the birefringence and the PdNSs size on w_{Me}. (a) Polarized photographs of heptane solutions used for products (Table S2). (b) Width and (c) thickness of the PdNSs.

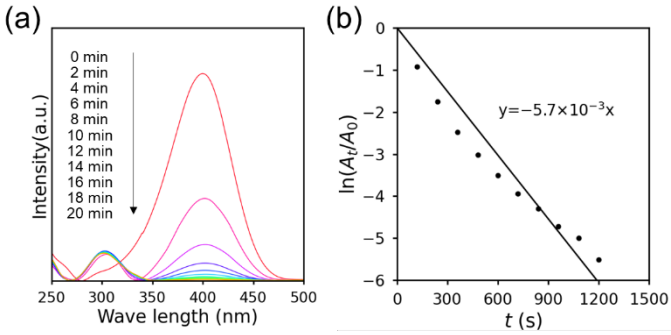

Fig. 5 Catalytic activity of PdNSs. (a) Successive UV–Vis spectra of the reduction of 4-NP in the presence of $NaBH_4$ using PdNSs as catalysts. (b) The relationship between $\ln([4\text{-NP}]/[4\text{-NP}]_0)$ and reaction time. The ratio of 4-nitrophenol ([4-NP] at time t) to its initial value $[4\text{-NP}]_0$ was directly obtained by the relative intensity of the respective absorbance A_t/A_0 with absorption peaks at 400 nm. The plots are fitted as a linear function with a slope $-k_{app}$ (solid line).

solutions. Although product **1** has shape anisotropy, it grows thicker than the others, and the standard deviation of the thickness is larger. It indicates that there are biaxial micelles whose thickness fluctuates, as shown in Fig. S5b.[41] As w_{Me} increases, the thickness of products **2**-**5** decreases and their width increases; their standard deviations are almost identical in this region. These results imply that methanol stabilizes the anisotropic shape of biaxial micelles, which are relatively monodispersed, as shown in Fig. S5c. We observed an opposite trend for products **9** and **10**. The trend of the size distribution of the PdNSs is ambiguous in DLS measurements that cannot evaluate the anisotropy of the particles, as shown in Fig. S6. We can conclude that the NS molding method enables us to evaluate the bilayers of small molecules that rapidly associate and dissociate in liquids.

We examined the catalytic activity of the obtained PdNSs to reduce 4-NP to 4-AP; this reaction is useful for the analysis of the catalytic performance using UV-visible spectroscopy, as shown in Fig. S7.[42] This reaction cannot proceed without a catalyst at room temperature.[43] We have already reported that the larger the width of NSs, the higher the catalytic performance.[28] Since we can expect the performance of the other products from that of one, we tested only product 6, which we had the largest amount. After adding the PdNSs into the 4-NP solution with an excess amount of $NaBH_4$, the intensity of the absorption peaks for 4-NP around 400 nm started decreasing along with a relative increase in the peak for 4-AP at 317 nm, as shown in Fig. 5a. Since we used an excessive amount of the reductant $NaBH_4$, the reaction is expected to be independent of $NaBH_4$ concentration. It can be simplified to

$$-\mathrm{d}[4\text{-NP}]/\mathrm{d}t = k_{app}\,[4\text{-NP}],$$

$$\ln([4\text{-NP}]/[4\text{-NP}]_0) = -k_{app}\cdot t,$$

where $[4\text{-NP}]$ and $[4\text{-NP}]_0$ are the concentrations of 4-nitrophenolate at the times t and 0, respectively. We can assume

$$\ln([4\text{-NP}]/[4\text{-NP}]_0) = \ln(A/A_0),$$

where A and A_0 are the corresponding absorbances of the typical band at 400 nm, respectively. We fitted a plot of $\ln(A/A_0)$ vs. reaction time, as shown in Fig. 5b. The linear correlation indicates that the above reaction is ruled by first-order kinetics, and the rate constant is 5.7×10^{-3} s^{-1}. These results should be compared with previously reported ones. The normalized rate constant (k_{nor}) was determined by

$$k_{nor} = k_{app}/(c[NaBH_4])$$

where k_{app} is normalized about the total amount of the catalyst (c) and the borohydride concentration ($[NaBH_4]$).[36] The k_{nor} value obtained for the PdNSs was 28287 g^{-1} s^{-1} M^{-1}. This value is greater than the k_{nor} estimated for other Pd catalysts without any supports, as shown in Table S3. This result should come from the increase in the relative surface area. The best catalyst is expected to be synthesized between the synthetic conditions for products 6 and 8.

Conclusions

We have successfully evaluated the dynamics of bilayers of the HL phase in TRAP solutions by observing PdNSs growing in the bilayers. The average and standard deviation of width and thickness of PdNSs depend on w_{Me}. These data have explained that the biaxiality of bilayers is statically important and the lateral association and dissociation of bilayers are dynamically important for stabilizing HL phases. This method can measure the size of such stimuli-sensitive bilayer structures in situ. Moreover, the PdNSs with a few nanometers of thickness and several hundred nanometers of width show higher catalytic activity for the reduction reaction of 4-NP to 4-AP than the previously reported Pd catalysts without any supports.

Conflicts of interest

There are no conflicts to declare.

Author contributions

KS performed the experiments, comprehensive study and manuscript drafting. JAHG and YT performed the experiments and developed the methodology. KM and NN performed the writing (review & editing). YU is the project leader of this work and supervises the work.

Acknowledgments

The authors thank Prof. T. Hirai and Prof. Y. Shiraishi for their help using a dynamic light scattering photometer. This work was supported in part by the Advanced Characterization Nanotechnology Platform, Nanotechnology Platform Program of the Ministry of Education, Culture, Sports, Science and Technology (MEXT), Japan, Grant Number JPMXP09A21OS0028 at the Research Center for Ultra-High Voltage Electron Microscopy (Nanotechnology Open Facilities) in Osaka University, and JSPS KAKENHI Grant Number JP22H04477 and JP22J10688.

Notes and references

1 R. D. Kornberg and H. M. McConnell, *Biochemistry*, 1971, **10**, 1111–1120.
2 P. Mueller, D. O. Rudin, H. T. Tien and W. C. Wescott, *Nature*, 1962, **194**, 979–980.
3 E. T. Castellana and P. S. Cremer, *Surf. Sci. Rep.*, 2006, **61**, 429–444.
4 M. Edidin, *Nat. Rev. Mol. Cell Biol.*, 2003, **4**, 414–418.
5 M. Bloom, E. Evans and O. Mouritsen, *Q. Rev. Biophys.*, 1991, **24**, 293–397.
6 S. Mura, J. Nicolas and P. Couvreur, *Nat. Mater.*, 2013, **12**, 991–1003.
7 M. J. Parnham and H. Wetzig, *Chem. Phys. Lipids*, 1993, **64**, 263–274.
8 M. J. Langton, *Nat. Rev. Chem.*, 2021, **5**, 46–61.
9 S. Ohki, S. Roy, H. Ohshima and K. Leonards, *Biochemistry*, 1984, **23**, 6126–6132.
10 P. E. G. Thorén, D. Persson, P. Lincoln and B. Nordén, *Biophys. Chem.*, 2005, **114**, 169–179.
11 T. Baba, L.-Q. Zheng, H. Minamikawa and M. Hato, *J. Colloid Interface Sci.*, 2000, **223**, 235–243.
12 H. Yin, Y. Lin, J. Huang and J. Ye, *Langmuir*, 2007, **23**, 4225–4230.
13 P. Marmottant, T. Biben and S. Hilgenfeldt, *Proc. R. Soc. A Math. Phys. Eng. Sci.*, 2008, **464**, 1781–1800.
14 F. J. Carrión, A. de la Maza and J. L. Parra, *J. Colloid Interface Sci.*, 1994, **164**, 78–87.
15 D.-W. Jeong, H. Jang, S. Q. Choi and M. C. Choi, *Sci. Rep.*, 2016, **6**, 38158.
16 B. Roy, P. Guha, R. Bhattarai, P. Nahak, G. Karmakar, P. Chettri and A. K. Panda, *J. Oleo Sci.*, 2016, **65**, 399–411.
17 C. Chen, D. Han, C. Cai and X. Tang, *J. Control. Release*, 2010, **142**, 299–311.
18 G. Bozzuto and A. Molinari, *Int. J. Nanomedicine*, 2015, **10**, 975–999.
19 X. Zhang, Y. Li, S. Shen, S. Lee and H. Dou, *Trends Anal. Chem.*, 2018, **108**, 231–238.
20 S. P. Damari, D. Shamrakov, M. Varenik, E. Koren, E. Nativ-Roth, Y. Barenholz and O. Regev, *Int. J. Pharm.*, 2018, **547**, 648–655.
21 D. Guimarães, A. Cavaco-Paulo and E. Nogueira, *Int. J. Pharm.*, 2021, **601**, 120571.
22 M.-P. Mingeot-Leclercq, M. Deleu, R. Brasseur and Y. F. Dufrêne, *Nat. Protoc.*, 2008, **3**, 1654–1659.
23 Y. Uchida, T. Nishizawa, T. Omiya, Y. Hirota and N. Nishiyama, *J. Am. Chem. Soc.*, 2016, **138**, 1103–1105.
24 T. Omiya, K. Sasaki, Y. Uchida and N. Nishiyama, *ACS Appl. Nano Mater.*, 2018, **1**, 3779–3784.
25 T. Omiya, K. Sasaki, Y. Uchida and N. Nishiyama, *Mol. Cryst. Liq. Cryst.*, 2019, **684**, 1–6.
26 K. Sasaki, T. Okue, T. Nakai, Y. Uchida and N. Nishiyama, *Langmuir*, 2021, **37**, 5872–5877.
27 K. Sasaki, T. Okue, Y. Shu, K. Miyake, Y. Uchida and N. Nishiyama, *Dalton Trans.*, 2021, **50**, 10394–10399.
28 K. Sasaki, K. Miyake, Y. Uchida and N. Nishiyama, *ACS Appl. Nano Mater.*, 2022, **5**, 4998–5005.
29 F. C. Larche, S. El Qebbaj and J. Marignan, *J. Phys. Chem.*, 1986, **90**, 707–710.
30 R. Strey, R. Schomäcker, D. Roux, F. Nallet and U. Olsson, *J. Chem. Soc. Faraday Trans.*, 1990, **86**, 2253–2261.
31 J. Yamamoto and H. Tanaka, *Phys. Rev. Lett.*, 1995, **74**, 932–935.
32 C. Amatore and A. Jutand, *Acc. Chem. Res.*, 2000, **33**, 314–321.
33 D. Gao, H. Zhou, J. Wang, S. Miao, F. Yang, G. Wang, J. Wang and X. Bao, *J. Am. Chem. Soc.*, 2015, **137**, 4288–4291.
34 E. Antolini, *Energy Environ. Sci.*, 2009, **2**, 915–931.
35 A. Kolmakov, D. O. Klenov, Y. Lilach, S. Stemmer and M. Moskovits, *Nano Lett.*, 2005, **5**, 667–673.
36 S. Mourdikoudis, V. Montes-García, S. Rodal-Cedeira, N. Winckelmans, I. Pérez-Juste, H. Wu, S. Bals, J. Pérez-Juste and I. Pastoriza-Santos, *Dalton Trans.*, 2019, **48**, 3758–3767.
37 Y. Zhang, M. Wang, E. Zhu, Y. Zheng, Y. Huang and X. Huang, *Nano Lett.*, 2015, **15**, 7519–7525.
38 H. Saravani, M. Farsadrooh, M. S. Mollashahi, M. Hajnajafi and A. S. Douk, *Int. J. Hydrogen Energy*, 2020, **45**, 21232–21240.
39 Y. Zhao, X. Tan, W. Yang, C. Jia, X. Chen, W. Ren, S. C. Smith and C. Zhao, *Angew. Chem. Int. Ed.*, 2020, **59**, 21493–21498.
40 F. Nosheen, N. Wasfi, S. Aslam, T. Anwar, S. Hussain, N. Hussain, S. N. Shah, N. Shaheen, A. Ashraf, Y. Zhu, H. Wang, J. Ma, Z. Zhang and W. Hu, *Nanoscale*, 2020, **12**, 4219–4237.
41 E. Akpinar, D. Reis and A. M. F. Neto, *Liq. Cryst.*, 2012, **39**, 881–888.
42 E. C. B. A. Alegria, A. P. C. Ribeiro, M. Mendes, A. M. Ferraria, A. M. Botelho do Rego and A. J. L. Pombeiro, *Nanomaterials*, 2018, **8**, 6–10.
43 Q. Ji, J. P. Hill and K. Ariga, *J. Mater. Chem. A*, 2013, **1**, 3600–3606.